























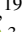






























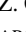








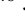

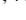



JWST NIRSpec+MIRI Observations of the nearby Type IIP supernova 2022acko

M. SHAHBANDEH ¹, C. ASHALL ², P. HOEFELICH ³, E. BARON ^{4,5,6}, O. FOX ¹, T. MERA ³, J. DERKACY ²,
M. D. STRITZINGER ⁷, B. SHAPPEE ⁸, D. LAW ¹, J. MORRISON ¹, T. PAULY ¹, J. PIEREL ¹, K. MEDLER ⁹, J. ANDREWS ¹⁰,
D. BAADE ¹¹, A. BOSTROEM ^{12,*}, P. BROWN ¹³, C. BURNS ¹⁴, A. BURROW ¹⁵, A. CIKOTA ¹⁶, D. CROSS ¹⁷, S. DAVIS ¹⁸,
T. DE JAEGER ¹⁹, A. DO ⁸, Y. DONG ²⁰, I. DOMINGUEZ ²¹, L. GALBANY ^{17,22}, D. JANZEN ²³, J. JENCSON ²⁴, E. HOANG ²⁵,
E. HSIAO ³, E. KARAMEHMETOGLU ⁷, B. KHAGHANI ², K. KRISCIUNAS ¹³, S. KUMAR ³, J. LU ³, M. LUNDQUIST ²⁶,
J. MAUND ²⁷, P. MAZZALI ^{9,28}, N. MORRELL ²⁹, F. PATAT ¹¹, J. PEARSON ¹², C. PFEFFER ², M. PHILLIPS ²⁹, A. REST ¹,
N. RETAMAL ²⁰, S. STANGL ¹⁵, M. SHRESTHA ¹², C. STEVENS ², N. SUNTZEFF ¹³, C. TELESCO ³⁰, M. TUCKER ^{31,†},
L. WANG ³², Y. YANG ³³, Y.-Z. CAI ^{34,35,36}, Y. CAMACHO-NEVES ³⁷, N. ELIAS-ROSA ³⁸, R. FOLEY ³⁹, S. JHA ³⁷, L. KWOK ³⁷,
C. LARISON ³⁷, N. LEBARON ³³, S. MORAN ⁴⁰, J. RHO ^{41,42}, I. SALMASO ^{43,44}, J. SCHMIDT ¹⁸ AND S. TINYANONT ⁴⁵

¹Space Telescope Science Institute, 3700 San Martin Drive, Baltimore, MD 21218-2410, USA

²Department of Physics, Virginia Tech, Blacksburg, VA 24061, USA

³Department of Physics, Florida State University, 77 Chieftan Way, Tallahassee, FL 32306, USA

⁴Planetary Science Institute, 1700 East Fort Lowell Road, Suite 106, Tucson, AZ 85719-2395, USA

⁵Hamburger Sternwarte, Gojenbergsweg 112, D-21029 Hamburg, Germany

⁶Dept of Physics & Astronomy, University of Oklahoma, 440 W. Brooks, Rm 100, Norman, OK USA

⁷Department of Physics and Astronomy, Aarhus University, Ny Munkegade 120, DK-8000 Aarhus C, Denmark

⁸Institute for Astronomy, University of Hawai'i at Manoa, 2680 Woodlawn Dr., Hawai'i, HI 96822, USA

⁹Astrophysics Research Institute, Liverpool John Moores University, UK

¹⁰Gemini Observatory/NSF's NOIRLab, 670 North A'ohoku Place, Hilo, HI 96720-2700, USA

¹¹European Organization for Astronomical Research in the Southern Hemisphere (ESO), Karl-Schwarzschild-Str. 2, 85748 Garching b. München, Germany

¹²Steward Observatory, University of Arizona, 933 North Cherry Avenue, Tucson, AZ 85721-0065, USA

¹³George P. and Cynthia Woods Mitchell Institute for Fundamental Physics and Astronomy, Texas A&M University, Department of Physics and Astronomy, College Station, TX 77843, USA

¹⁴Observatories of the Carnegie Institution for Science, 813 Santa Barbara Street, Pasadena, CA 91101, USA

¹⁵Homer L. Dodge Department of Physics and Astronomy, University of Oklahoma, 440 W. Brooks, Rm 100, Norman, OK 73019-2061, USA

¹⁶Gemini Observatory/NSF's NOIRLab, Casilla 603, La Serena, Chile

¹⁷Institute of Space Sciences (ICE, CSIC), Campus UAB, Carrer de Can Magrans, s/n, E-08193 Barcelona, Spain

¹⁸Private Astronomer

¹⁹LPNHE, (CNRS/IN2P3, Sorbonne Université, Université Paris Cité), Laboratoire de Physique Nucléaire et de Hautes Énergies, 75005, Paris, France

²⁰Department of Physics, University of California, 1 Shields Avenue, Davis, CA 95616-5270, USA

²¹Universidad de Granada, 18071, Granada, Spain

²²Institut d'Estudis Espacials de Catalunya (IEEC), E-08034 Barcelona, Spain

²³Department of Physics and Engineering Physics, University of Saskatchewan, 116 Science Place, Saskatoon, SK S7N 5E2, Canada

²⁴Department of Physics and Astronomy, The Johns Hopkins University, 3400 North Charles Street, Baltimore, MD 21218, USA

²⁵Department of Physics and Astronomy, University of California, Davis, 1 Shields Avenue, Davis, CA 95616-5270, USA

²⁶W. M. Keck Observatory, 65-1120 Māmalahoa Highway, Kamuela, HI 96743-8431, USA

²⁷Department of Physics and Astronomy, University of Sheffield, Hicks Building, Hounsfield Road, Sheffield S3 7RH, U.K.

²⁸Max-Planck Institute for Astrophysics, Garching, Germany

²⁹Las Campanas Observatory, Carnegie Observatories, Casilla 601, La Serena, Chile

³⁰Department of Astronomy, University of Florida, Gainesville, FL 32611 USA

³¹Center for Cosmology and AstroParticle Physics, The Ohio State University, 191 W. Woodruff Ave., Columbus, OH 43210, USA

³²Department of Physics and Astronomy, Texas A&M University, College Station, TX 77843, USA

³³Department of Astronomy, University of California, Berkeley, CA 94720-3411, USA[‡]

³⁴Yunnan Observatories, Chinese Academy of Sciences, Kunming 650216, PR China

³⁵Key Laboratory for the Structure and Evolution of Celestial Objects, Chinese Academy of Sciences, Kunming 650216, PR China

³⁶International Centre of Supernovae, Yunnan Key Laboratory, Kunming 650216, P.R. China

³⁷Department of Physics and Astronomy, Rutgers, the State University of New Jersey,

136 Frelinghuysen Road, Piscataway, NJ 08854-8019, USA

³⁸INAF - Osservatorio Astronomico di Padova, Vicolo dell'Osservatorio 5, 35122, Padova, Italy

³⁹Department of Astronomy and Astrophysics, University of California, Santa Cruz, CA 95064-1077, USA

⁴⁰Department of Physics and Astronomy, University of Turku, Vesilinnantie 5, FI-20500, Finland

⁴¹SETI Institute, 339 N. Bernardo Ave., Ste. 200, Mountain View, CA 94043, USA

⁴²Department of Physics and Astronomy, Seoul National University, Gwanak-ro 1, Gwanak-gu, Seoul, 08826, South Korea

⁴³Dipartimento di Fisica e Astronomia "G. Galilei", Università degli Studi di Padova, Vicolo dell'Osservatorio 3, 35122, Padova, Italy

⁴⁴INAF - Osservatorio Astronomico di Padova, Vicolo dell'Osservatorio 5, 35122, Padova, Italy

⁴⁵National Astronomical Research Institute of Thailand, 260 Moo 4, Donkaew, Maerim, Chiang Mai 50180, Thailand

(Received XXX; Revised January 29, 2024; Accepted xxx)

Submitted to ApJL

ABSTRACT

We present *JWST* spectral and photometric observations of the Type IIP supernova (SN) 2022acko at ~ 50 days past explosions. These data are the first *JWST* spectral observations of a core-collapse SN. We identify ~ 30 different H I features, other features associated with products produced from the CNO cycle, and s-process elements such as Sc II, Ba II. By combining the *JWST* spectra with ground-based optical and NIR spectra, we construct a full Spectral Energy Distribution from 0.4 to 25 μm and find that the *JWST* spectra are fully consistent with the simultaneous *JWST* photometry. The data lack signatures of CO formation and we estimate a limit on the CO mass of $< 10^{-8} M_{\odot}$. We demonstrate how the CO fundamental band limits can be used to probe underlying physics during the stellar evolution, explosion, and the environment. The observations indicate little mixing between the H envelope and C/O core in the ejecta and show no evidence for dust. The data presented here set a critical baseline for future *JWST* observations, where possible molecular and dust formation may be seen.

Keywords: supernovae: general - supernovae: individual (SN 2022acko), *JWST*

1. INTRODUCTION

The origin of the substantial quantities of dust inferred from submillimeter and millimeter observations of high-redshift (z) quasars is an unsolved astrophysical question (e.g., Bertoldi et al. 2003; Priddey et al. 2003; Li et al. 2020). In the local Universe, most dust is believed to originate during the evolutionary phase of low- and intermediate-mass stars when they reach the asymptotic giant branch on the Hertzsprung-Russell diagram (e.g., González Delgado et al. 2003; Ferrarotti & Gail 2006). However, at higher redshifts (i.e., $z > 6.3$), alternative processes occurring on shorter time scales are more likely at play.

For more than half a century, core-collapse supernovae (CCSNe) have been proposed as a potential source of dust (Cernuschi et al. 1967; Hoyle & Wickramasinghe 1970). In particular, hydrogen-rich CCSNe known as Type II plateau supernovae (hereafter, SNe IIP), are linked to the demise of massive stars born with initial masses ranging between 8 to 25 M_{\odot} , and with lifetimes of less than 50 Myrs. SNe IIP have

played a significant role in the evolution of the Universe, contributing significantly to the production of heavy elements, and the genesis of dust, both locally and at cosmologically significant redshifts (e.g., Maiolino et al. 2004; Schneider et al. 2004; Dwek et al. 2007; Nozawa et al. 2008; Gall et al. 2011). Models of the expanding SN ejecta have demonstrated their ability to condense sufficient quantities (0.1–1 M_{\odot}) of dust (e.g., Todini & Ferrara 2001; Nozawa et al. 2003; Cherchneff & Dwek 2009; Sarangi & Cherchneff 2015; Sluder et al. 2018; Sarangi et al. 2018).

Only a handful of SNe IIP have been documented to form dust, and until recently, these cases produced 2–3 orders of magnitude less dust than predicted by modeling. The prerequisite for the genesis of dust is the creation of molecules, which serve both as a coolant and as a nucleation site. In SNe IIP, the order of the formation of silicon-monoxide (*SiO*) versus carbon-monoxide (*CO*) can be dependent upon the initial zero-age main sequence (ZAMS) mass of the progenitor stars since it leads to differing amounts of C, O, and Si in the stars at the time of their demise (Woosley et al. 2002).

The majority of previous studies on molecular formation in CCSNe have concentrated on searching for the ($\approx 2.3 \mu\text{m}$) CO first overtone feature. Evidence of molecular formation

* LSSTC Catalyst Fellow

† CCAPP Fellow

‡ Bengier-Winslow-Robertson Postdoctoral Fellow

was first found in data of SN 1987A (e.g., Catchpole et al. 1988; Meikle et al. 1989; Wooden et al. 1993), and to date has also been identified in around a dozen SNe IIP (e.g., Aitken et al. 1988; Kotak et al. 2005a; Meikle et al. 2007a; Kotak et al. 2009; Fox et al. 2010; Tinyanont et al. 2019; Szalai et al. 2019; Davis et al. 2019).

The ability to observe the CO and SiO fundamental bands began to improve with the advent of the *Spitzer Space Telescope* (*SST*), as the longer spectral wavelength range was particularly well-suited for studying molecular formation in CCSNe. *SST* spectra of SN 2005af showed indications of SiO formation (Kotak et al. 2006), while observations of SN 2004dj contained the red part of the CO fundamental band (Kotak et al. 2005b). Given the nature of the data, these initial assessments of molecules in a handful of SNe left open the question of whether we see pre-existing or freshly synthesized dust (Gerardy et al. 2000).

The *James Webb Space Telescope* (*JWST*) has revolutionized the communities ability to accurately study molecule and dust formation in various types of SNe. Recently, Shahbandeh et al. (2023) used *JWST* Mid-Infrared Instrument (MIRI; Bouchet et al. 2015; Ressler et al. 2015; Rieke et al. 2015, 2022) observations of the Type IIP SN 2004et to infer a dust mass lower limit of $0.014 M_{\odot}$. This exceeds estimates estimated from Mid-infrared (MIR) observations of all other observed SNe IIP (see Shahbandeh et al. 2023), and highlights the potential of SNe IIP being a major contributor to the dust content of the Universe.

While deep imaging is possible, *JWST* spectroscopy offers additional insights into the explosion physics of CCSNe. Near-infrared (NIR) and MIR spectroscopic time series covering the duration of a CCSN’s lifetime can provide information on the formation of molecules like CO and SiO . To fully understand how SNe IIP produces molecules and dust, we must follow them beginning soon after exploding and over the duration of many decades. Where early data allows us to set a baseline for any pre-existing molecular and dust formation.

We present Near-Infrared Spectrograph (NIRSpec; Jakobsen et al. 2022) and MIRI observations of the Type IIP SN 2022acko, as part of *JWST* GO-2122 (PI: C. Ashall), which aims to follow the evolution of a single SN IIP from the early H recombination driven plateau phase thru late times when CO and SiO molecules form. Here, we present the first NIRSpec+MIRI spectral observation from this program, the first CCSN spectrum obtained with *JWST*. We also present near-simultaneous optical and NIR ground-based spectral observations of SN 2022acko, as well as serendipitous multi-band imaging obtained by the Physics at High Angular Resolution of Nearby Galaxies (PHANGS) *JWST* Cycle 1 Treasury Program (Lee et al. 2023).

Our goals are to *i*) measure the level of mixing within the ejecta by searching for CO formation, trace the elements

Table 1. SN 2022acko details.

Parameter	Value	Reference
RA	03:19:38.99	Lundquist et al. (2022)
Dec	−19:23:42.68	Lundquist et al. (2022)
Redshift	0.00526	Bostroem et al. (2023)
Host galaxy	NGC 1300	Lundquist et al. (2022)
$E(B - V)_{MW}$	0.026 ± 0.001 mag	Bostroem et al. (2023)
$E(B - V)_{host}$	0.04 ± 0.01 mag	Bostroem et al. (2023)
Distance [Mpc]	19.0 ± 2.9	Anand et al. (2021)
Explosion epoch (t_{exp} ; MJD) ^a	59918.17 ± 0.4	Bostroem et al. (2023)

of the CNO-cycle, and identify possible s-process elements, *ii*) set limits for pre-existing molecules and dust in the interstellar medium (ISM) and circumstellar medium (CSM), and *iii*) demonstrate the importance of fundamental bands of molecules, obtain values and tight upper limits for the nearby environment, for mixing processes during the stellar evolution, and for the physics of the explosion. This is a key to being able to separate pre-existing molecules and dust from newly formed products, and to evaluate the SN IIP as dust-producers in the early Universe.

SN 2022acko was discovered on 2022 December 06.2 UT (i.e., MJD-59919.2) by the Distance Less Than 40 Mpc Survey (DLT40; Tartaglia et al. 2018), and a spectrum obtained 12 hours with the Lijiang 2.4-m telescope showed it to be a young SN IIP (Li et al. 2022). With J2000 coordinates R.A. = $03^h 19^m 38^s.99$ and Decl. = $-19^{\circ} 23' 42''.68$, the location of SN 2022acko is 0.0181° North-West from the center of NGC 1300 (de Vaucouleurs et al. 1991). According to the NASA extragalactic database (NED) the heliocentric redshift (z) to the host-galaxy of SN 2022acko is $z = 0.00526$. In the following, we adopt the tip of red giant branch (TRGB) distance measurement from the PHANGS team of 18.99 ± 2.85 Mpc (Anand et al. 2021).

Its proximity as well as the location of SN 2022acko outside the core of its host made it an ideal target for our *JWST*-GO-2122 ToO program (PI: C. Ashall, DOI:10.17909/ea3g-5z06). Ultraviolet and optical observations of SN 2022acko indicate it is a low-luminosity SN IIP (see Bostroem et al. 2023). For consistency, throughout this work, we adopt the same basic parameters for SN 2022acko as inferred by Bostroem et al. (see Table 1), including their preferred reddening values and estimated explosion epoch which they demonstrated likely occurred within 24 hours prior to discovery.

The outline of this paper is as follows. Our observations of SN 2022acko are presented in Section 2, which is then followed by the identification of key spectral features and data

comparisons in Section 3. Next in Section 4, H line velocities are measured, after which the full optical-to-MIR spectral energy distribution (SED) constructed in Section 5. Limits on pre-existing molecular and dust formation are determined in Section 6, and then in Section 7, SN 2022acko is compared with SN 1987A in order to understand the amount of mixing in the ejecta. Finally, a summary of the results and our conclusions are given in Section 8.

2. OBSERVATIONS

2.1. NIRC*am* and MIRI Imaging

PHANGS obtained imaging of NGC 1300 with NIRC*am* and MIRI on 59969.74 MJD (51.57 days post-explosion), which is within ~ 1 day of our programme’s NIRS*pec* observations of SN 2022acko (see below). This data was acquired in four NIR filters (i.e., *F200W*, *F300M*, and *F335M*, *F360M*), as well as in four MIR filters (i.e., *F770W*, *F1000W*, *F1130W*, and *F2100W*) providing a measure of SN 2022acko’s Spectral Energy Distribution (SED) between ~ 1.7 – 21.0 μm . Calibrated level 2 data products were downloaded from the Mikulski Archive for Space Telescopes (MAST), from which point-spread function (PSF) photometry was computed.

A color-stacked image constructed from MIRI images is presented in Fig. 1. The position of SN 2022acko at the top of the image is indicated with a red circle while a 10×10 arcsec zoom of this region is provided in the bottom-right inset. SN 2022acko is located in a region of star formation. Figure 2 shows the SN in a 30 by 30 pixel stamp in the *F300M*, *F355M*, *F360M*, *F770W*, *F1000W* and *F1130W* filters. The SN is clearly visible in each of these bands.

PSF photometry was computed using a custom-made python notebook making use of the *WebbPSF* photometry package (Perrin et al. 2014).¹ Various PSF sizes were used to ensure that the full variation within the data was encapsulated. The final magnitude was taken as the average flux across all fits, which have a residual less than 15%. The fluxes of all four dithers of each filter were then averaged, and the error in the flux was obtained using the standard deviation of the fluxes. A log of the photometric observations and the flux at these epochs, can be found in Table 2.

2.2. NIRS*pec*

We obtained a NIRS*pec* spectrum ($R \sim 1000$) of SN 2022acko from ~ 1.7 – 5.2 μm . The spectrum was acquired using the S400A1 slit, the G235M and G395M gratings, with the F170P and F290LP filters, respectively. The instrument setup had one exposure per grating and a total exposure time of 467.65 s. The details of the observational setup can be seen in Table 3. The data were taken on MJD 59968.4 at 50.2 d

Table 2. Log of *JWST* photometric observations. The average time of photometric observation is 51.6 d after the inferred time of the explosion.

Filters	Obs. date [MJD]	Exp. time [s]	Mag [mag]
<i>F200W</i> ^a	59969.82	215	17.00 ± 0.09 ^C
<i>F300M</i> ^a	59969.79	387	17.53 ± 0.03
<i>F335M</i> ^a	59969.80	387	17.60 ± 0.05
<i>F360M</i> ^a	59969.77	215 ^d	17.62 ± 0.01
<i>F770W</i> ^b	59969.65	88.8	18.63 ± 0.01
<i>F1000W</i> ^b	59969.66	122	19.19 ± 0.01
<i>F1130W</i> ^b	59969.66	311	19.35 ± 0.01
<i>F2100W</i> ^b	59969.68	322	$\leq 21.43 \pm \dots$

NOTE—^aNIRC*am* data, ^bMIRI data. All photometric observations were performed with a 4-point dither. ^C The *F200W* images were saturated in all exposures, therefore the photometry is highly uncertain. All exposure times are reported from four dithers unless otherwise stated.

past explosion. The observation consisted of a three-point dither pattern. The background-subtracted level-two spectra were combined into a single calibrated spectrum for each filter. The spectra were processed with the *JWST* Calibration Pipeline version 1.8.2, using the Calibration Reference Data System version 11.16.14 (Bushouse et al. 2023).

2.3. MIRI Medium Resolution Spectroscopy

Medium resolution spectroscopy (MRS) data were obtained with the MIRI instrument on *JWST*. Observations were taken in the Short, Medium, and Long gratings to ensure continuous wavelength coverage (5 – 25 μm) and stitched together. We note that the data longward of 15 μm is dominated by noise and instrumental thermal background; this is in part because of the scientific goals of these observations were to cover the *SiO* fundamental overtone at ~ 8.1 μm , the exposure time was not optimized for the longest wavelengths, and because of the known issues with the degrading count rate throughput of Ch3 and Ch4². The MRS data were reduced using a custom-built pipeline³ designed to extract point source observations with highly varying and/or complex backgrounds from MRS data cubes. The pipeline creates a master background based on 48 different positions in the data cube. This master background is then subtracted from the whole data cube before the aperture photometry is performed along the data cube, using the `EXTRACT1DSTEP` in stage 3 of the *JWST* reduction pipeline. The reduction shown here utilized version 1.12.1 of the *JWST*

¹ https://github.com/orifox/psf_phot/blob/main/space_phot/MIRI/miri_1028.ipynb

² <https://www.stsci.edu/contents/news/jwst/2023/miri-mrs-reduced-count-rate-update>

³ https://github.com/shahbandeh/MIRI_MRS

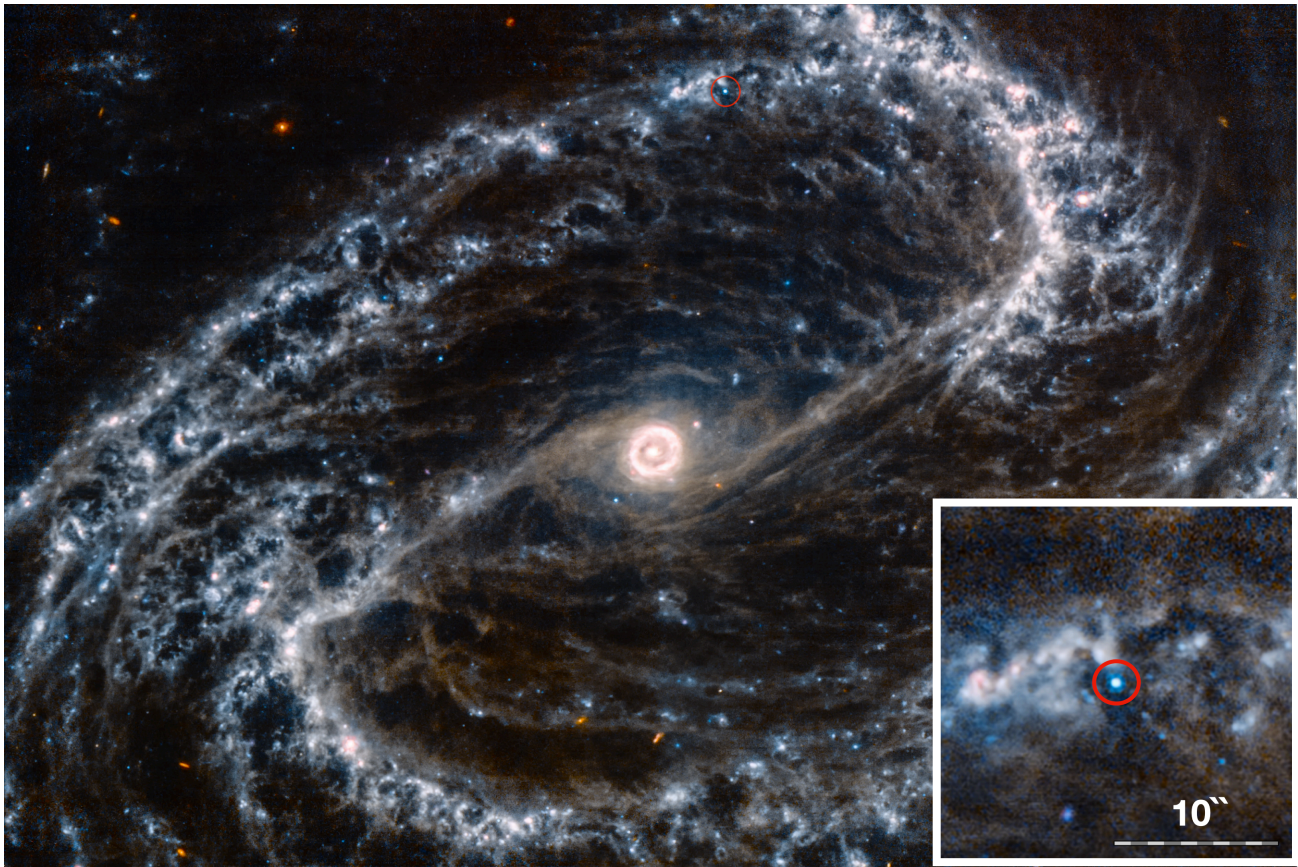


Figure 1. A color image of NGC 1300 constructed from three *JWST* MIRI images. The color code of the images are as follows, Red: *F2100W*, Orange: *F1130W*, Cyan: *F770W*. SN 2022acko is located in the top of the image in the red circle. A 10'' by 10'' inset around the location of the SN is seen in the bottom right. The SN is located in an area of star formation. The full resolution of this image can be found [here](#).

Calibration pipeline (Bushouse et al. 2023) and Calibration Reference Data System files version 11.17.1. Figure 3 shows the stacked MRS data cubes in each channel before and after background subtraction, and the spectrum is shown in full in Figure 6. The raw data associated with this reduction can be found at DOI:10.17909/ea3g-5z06.

2.4. Ground-based spectroscopy

To complete the SED to shorter wavelengths, we also present ground-based spectra of SN 2022acko at similar epochs. A summary of these optical and NIR observations is provided in Table 1.

An optical spectrum was obtained with the NUTS2 collaboration using the 2.54-m Nordic Optical Telescope (NOT) equipped with the Alhambra Faint Object Spectrograph and Camera (ALFOSC). The spectrum was taken on MJD 59978.86 which corresponds to +60.7 days post-explosion. The data were reduced within the PyRAF environment using the NUTS2 pipeline written by E. Cappellero.

A NIR spectrum was taken on MJD 59951.95 at +33.78 days post-explosion with the Near-Infrared Echellette Spectrometer (NIRES) mounted to the 10-m Keck II telescope. SN 2022acko was observed at two positions along the

slit (AB pairs) to perform background subtraction. An A0V star was observed immediately adjacent to the science observation, and used for both telluric and flux calibration. The NIRES data were reduced using the PYTHON-based `pypeit` package. Combining these four spectra produces the first-ever nearly-continuous spectral coverage between $\sim 0.4\text{--}25\ \mu\text{m}$, which demonstrates the power of combining ground-based and *JWST* data.

Two additional spectra were taken using the ALFOSC on the NOT via the NUTS collaboration, and an additional ground-based NIR spectrum was taken with EMIR mounted on the Gran Telescopio Canarias (GTC). These data are included in the online supplementary material.

3. LINE IDENTIFICATIONS AND DATA COMPARISON

The following section discusses the spectral lines contributing to the spectral formation. The spectra of SN 2022acko are taken towards the end of the plateau phase. The hydrogen (H) spectral series, including the Balmer, Paschen, Brackett, Pfund, and Humphreys dominate the spectra of SN 2022acko. We also see some features of heavier elements (e.g., Mazzali et al. 1992). Table 4 lists all of the spectral lines that have

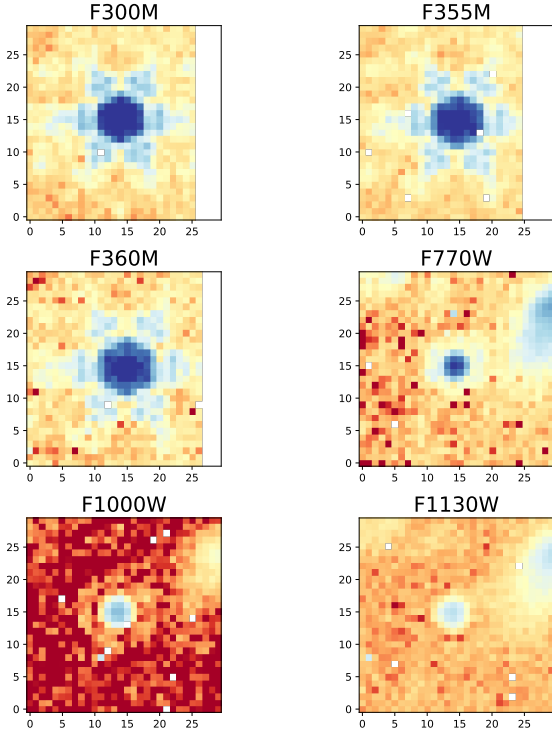


Figure 2. NIRCAM $F300M$, $F355M$, $F360M$ 30 pixel \times 30 pixel stamps of SN 2022acko, and MIRI $F770W$, $F1000W$ and $F1130W$ 30 pixel \times 30 pixel stamps of SN 2022acko. We do not show the $F2100W$ filter as the SN is not visible.

been identified in the full spectrum, and below, we discuss the line identifications within various regions.

3.1. Optical Spectrum

The top panel of Fig. 4 shows the optical spectrum of SN 2022acko. For assistance with line IDs we use the models from Baron et al. (2003). In the optical SN 2022acko is dominated by the Balmer series with some Paschen series: H_α (0.6563 μm), H_β (0.4861 μm), H_γ (0.4340 μm), H_δ (0.4102 μm), Pa_η (0.901 μm), Pa_ζ (0.923 μm), and Pa_ϵ (0.955 μm). Other ions which contribute to the spectral line formation include: the Ca II H&K lines (0.3933 μm , 0.3968 μm) and Ca II NIR triplet (0.8498 μm , 0.8542 μm , 0.8662 μm), Mg II 0.9218 μm , Na I 0.5896 μm , 0.5890 μm , Sc II 5527 μm , 5698 μm , 6280 μm , Ba II 6142 μm , and many lines of Fe II including 0.4359 μm , 0.4642 μm , 0.4862 μm , 0.4924 μm , 0.5018 μm , and 0.5169 μm . As well as C I lines particularly the line at 0.94 μm , just redward of Pa_ζ .

3.2. NIR ground-based spectrum

We use the lines IDs from Davis et al. (2019) and Shahbandeh et al. (2022) to assist us with identifying the main lines which contribute to the ground-based NIR spectrum. With the exception of Pa_α , which is located in the NIRSpec data, the H features in the ground-based NIR spectrum are dominated

Table 3. SN 2022acko spectral log.

Parameter	Value	Value	Value
MIRI/MRS Spectra			
Grating	Short	Medium	Long
Groups per Integration	36	36	36
Integrations per Exp.	1	1	1
Exposures per Dither	1	1	1
Total Dithers	4	4	4
Exp Time [s]	3440.148	3440.148	3440.148
Resolution ^a	~2,700		
Epoch ^a [days]	55.57		
T_{obs} [MJD]	59973.74		
NIRSpec Acquisition Image			
Filter	CLEAR
Exp Time [s]	0.08
Readout Pattern	NRSRAPID
NIRSpec Spectra			
Slit	S400A1	S400A1	...
Filter	F170P	F290LP	...
Groups per Integration	5	7	...
Integrations per Exp.	2	2	...
Exposures per Dither	1	2	...
Total Dithers	3	3	...
Exp Time [s]	196.43	271.22	...
Epoch ^a [days]	50.18	50.19	...
T_{obs} [MJD]	59968.35	59968.36	...
NIR Spectra/Keck-NIRES			
Exp time [s]	1200
T_{obs} [MJD]	59951.95
Epoch ^a [days]	33.78
Total Dithers	4
Slit width	0.5''
Optical Spectra/NOT-ALFOSC			
Exp time [s]	1800
T_{obs} [MJD]	59978.86
Epoch ^a [days]	60.69
Grism	Grism_#4
Slit width	1.0''

NOTE—^a Rest frame days relative to time of explosion, MJD = 59918.17 (Bostroem et al. 2023).

by the Paschen series. These include Pa_β (0.1282 μm), Pa_γ (0.1094 μm), and Pa_δ (0.1005 μm). Other lines identified in this spectrum are Sr II 1.0040 μm , 1.0330 μm , O I 1.1290 μm , Mg II 1.0092, 1.0927 μm , Ca II 1.1839 μm , 1.1950 μm , and C I 1.0694 μm , 1.1333 μm , 1.175 μm .

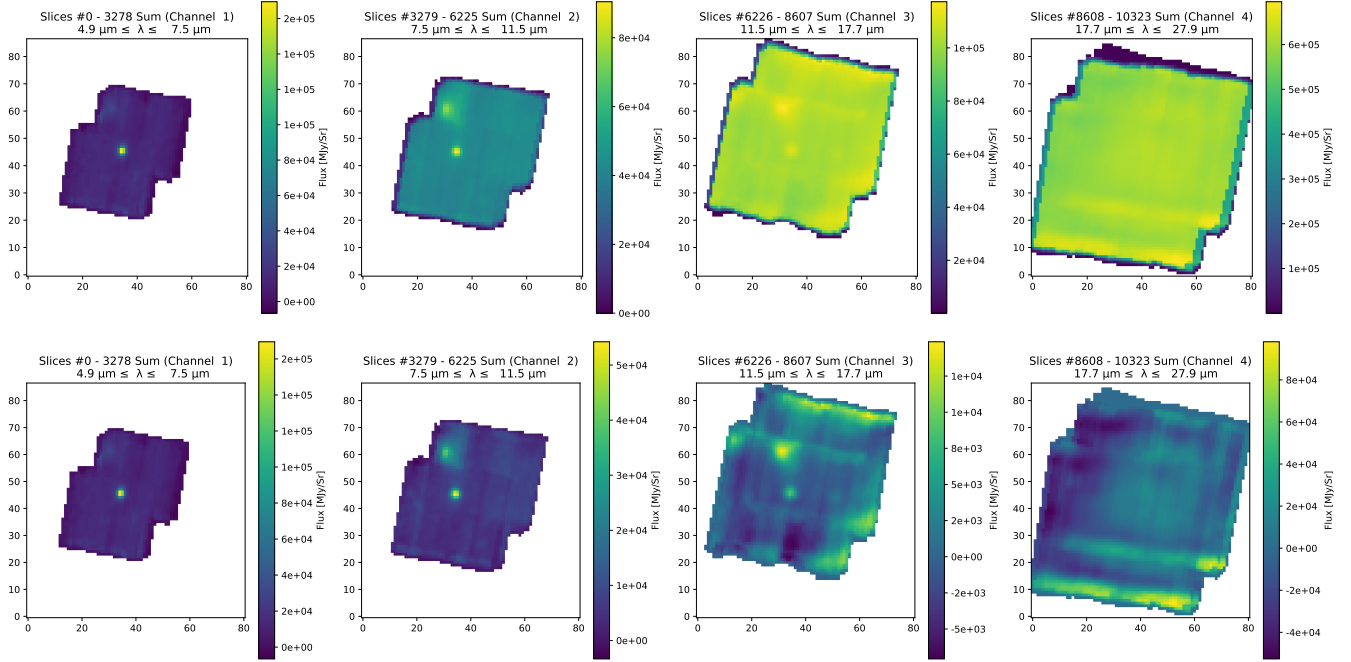


Figure 3. *Top panel:* MIRI/MRS cube of SN 2022acko before background subtraction divided separate by channel. Each channel is a collapsed sum of all its slices. *Bottom panel:* MIRI/MRS cubes of SN 2022acko after background subtraction.

3.3. NIR JWST/NIRSpec spectrum

Figure 5 shows the NIRSpec spectrum obtained at $\sim +50$ d. The spectrum is dominated by P Cygni profiles of H lines mainly coming from the Brackett and Pfund series. The main lines in the spectra include Br_{ϵ} (1.817 μm), H I 1.875 μm , Br_{δ} (1.944 μm), Br_{γ} (2.166 μm), Br_{β} (2.626 μm), H I 2.873 μm , 3.297 μm , 3.741 μm , Br_{α} (4.052 μm), H I 4.377 μm , Pf $_{\beta}$ (4.653 μm), H I 5.129 μm .

3.4. MIR JWST/MIRI spectrum

Figure 6 shows the lines identified in the MIRI spectrum. The MIRI spectrum is comprised of observations across four channels, which range from 4.90-7.65 μm for Channel 1, 7.51-11.70 μm for Channel 2, 11.55-17.98 μm for Channel 3, and 17.70-27.90 μm for Channel 4. Visual inspection of the non-background subtracted data cubes shows there is clear SN flux in the first two channels; the signal-to-noise (S/N) of the SN varies between 20 and 2 from 4.90-11.70 μm , after background subtraction, this S/N increases to 35 to 6 (see Figure 3). This gives us confidence that our line identifications shortwards of 11.70 μm are accurate. Before background subtraction, in Channel 3, the S/N varies from 1-2 depending on the exact wavelength range. After background subtraction, the S/N is ~ 3 . Due to the high background and low throughput of MIRI-MRS in channel 4, visual inspection of the pre-background subtracted data shows no sign of the SN. However, after background subtraction, (i.e. when the data is fully reduced using our pipeline) the supernova is visible in Channel 4 at a S/N of 1-3. For example, we clearly see

the SN at wavelength 22.167 μm , 25.1854 μm , 26.9623 μm . Therefore, we still choose to identify possible spectral lines in this region but as we could not manually inspect every wavelength slice for possible SN signal, we want to remind the reader that the identifications in this Channel are tentative.

Generally, the MIR spectrum is dominated by H lines (transitions from levels 6, 7, 8, and 9), however, there are several features that are from other ions. Some of the most notable spectral features include C II 5.539, 5.836, 6.775, 6.900 μm , N II 8.439, N III 9.175, 9.191 μm , O I 7.720, 10.384 μm and O II 9.332, 9.439 μm . The observation of s-process elements and lines of C, N, and O in the hydrogen elements validate our understanding of CNO burning during stellar evolution.

3.5. Spectral Comparison

In this section, we examine the differences between SN 2022acko and other CCSN which have MIR spectra. Figure 7 shows a comparison of the Spitzer Space Telescope data of SN 2005af obtained at day +67 (Kotak et al. 2006) with that of SN 1987A at day +56 (Aitken et al. 1988) and the MIRI/MRS data of SN 2022acko obtained at day +56 d. The three SNe are generally similar but have a few notable differences. At this epoch, SN 2022acko is still on the plateau phase and is dominated by H features, whereas SN 2005af was faster evolving and passed the plateau phase by day +67 (Kotak et al. 2005b). In fact, the forbidden lines identified by Kotak et al. (2006) are absent in both SN 1987A and SN 2022acko. Although the SN 2022acko MIRI spectrum

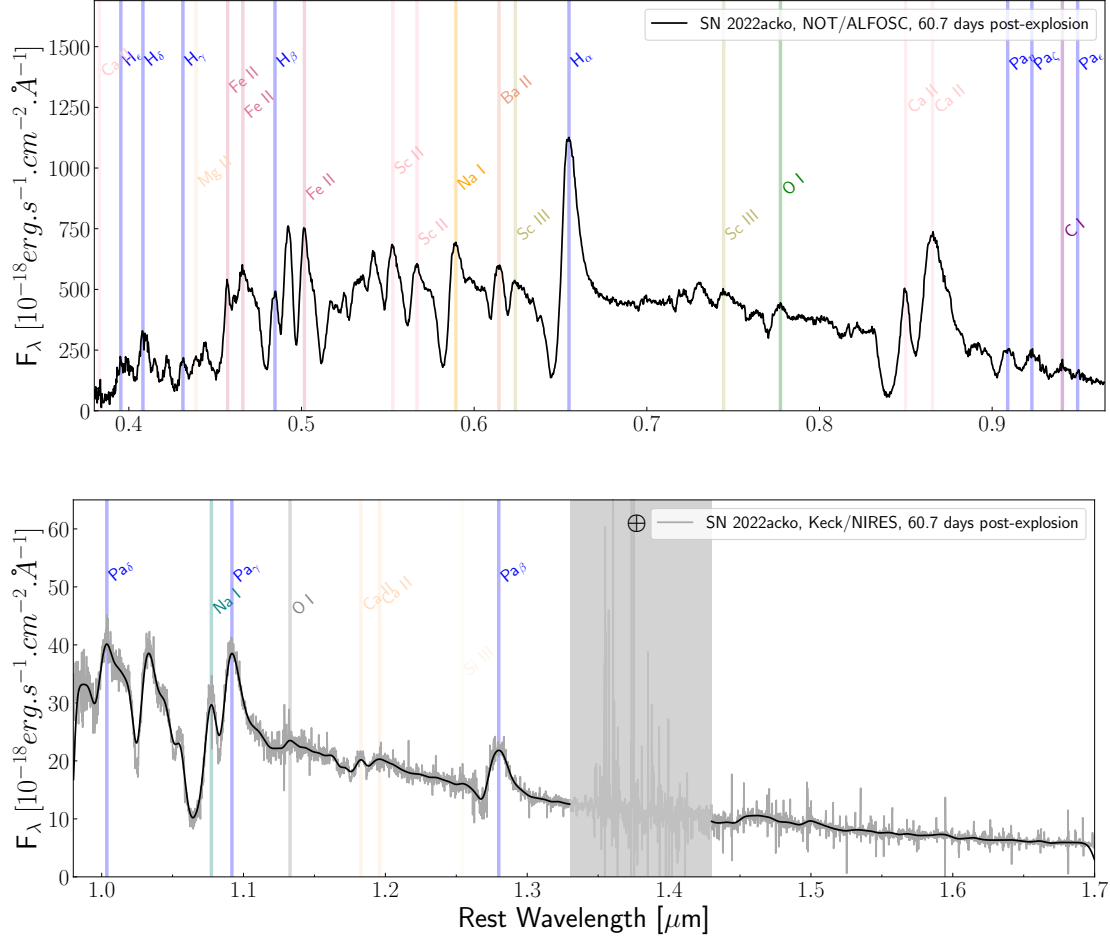


Figure 4. *First:* NOT (+ ALFOSC) optical spectrum of SN 2022acko, with labeled line IDs. *Second:* The Keck-II (+ NIRES) NIR spectrum with labeled line IDs.

is ~ 10 days earlier than SN 2005af, it appears to be evolving more slowly, thus we would expect the ZAMS mass of SN 2022acko to be larger than that of SN 2005af. SN 2004dj was also observed by the *SST* at epochs of 89–129 days (Kotak et al. 2005b). In this spectra [Ni II] lines were seen and the presence of *CO* was inferred as early as 106 days. Future observations of SN 2022acko will allow us to compare the epoch of *CO* formation, and evolution of the onset of forbidden lines, which will enable us to determine if SN 2022acko had a larger ejecta mass.

4. HYDROGEN VELOCITIES

To understand where in the ejecta the line formation of H is occurring we examine the profiles of all of the H lines in velocity space. Figure 8 shows the velocity profiles of Hydrogen from 0.4–25 μm . Overall, we see evidence for ~ 30 different spectral lines. Where four are from the ground-based optical spectrum, three are from the ground-based NIR, 11 are from the JWST NIRSpec data, and 11 are from the JWST MIRI spectrum. To determine the velocity of each

absorption, each H-profile was fit with a Gaussian function using the method described in (Shahbandeh et al. 2022). The H absorptions vary in velocity from 2100 to 4900 km s^{-1} ; see Table 4. The velocities of the H lines are strongly dependent on the transition, whereas the lower atomic transitions have increasingly higher velocities, see Fig. 9. We also note that for all the H P-Cygni features, the emissions of the profiles are blue-shifted by 1000–2000 km s^{-1} ; this is to be expected because the extended atmosphere will block parts of the red-shifted emission.

5. FULL SPECTRAL ENERGY DISTRIBUTION

By combining all of the spectra, we can produce the first 0.4 to 25 μm SED of a SN IIP, see Fig. 10. The average time of the SED is at ~ 52 d past explosion. For orientation, we characterize the overall energy distribution by the temperature of the black body. This is possible because Thomson and free-free emission dominate the NIR and MIR continuum. When

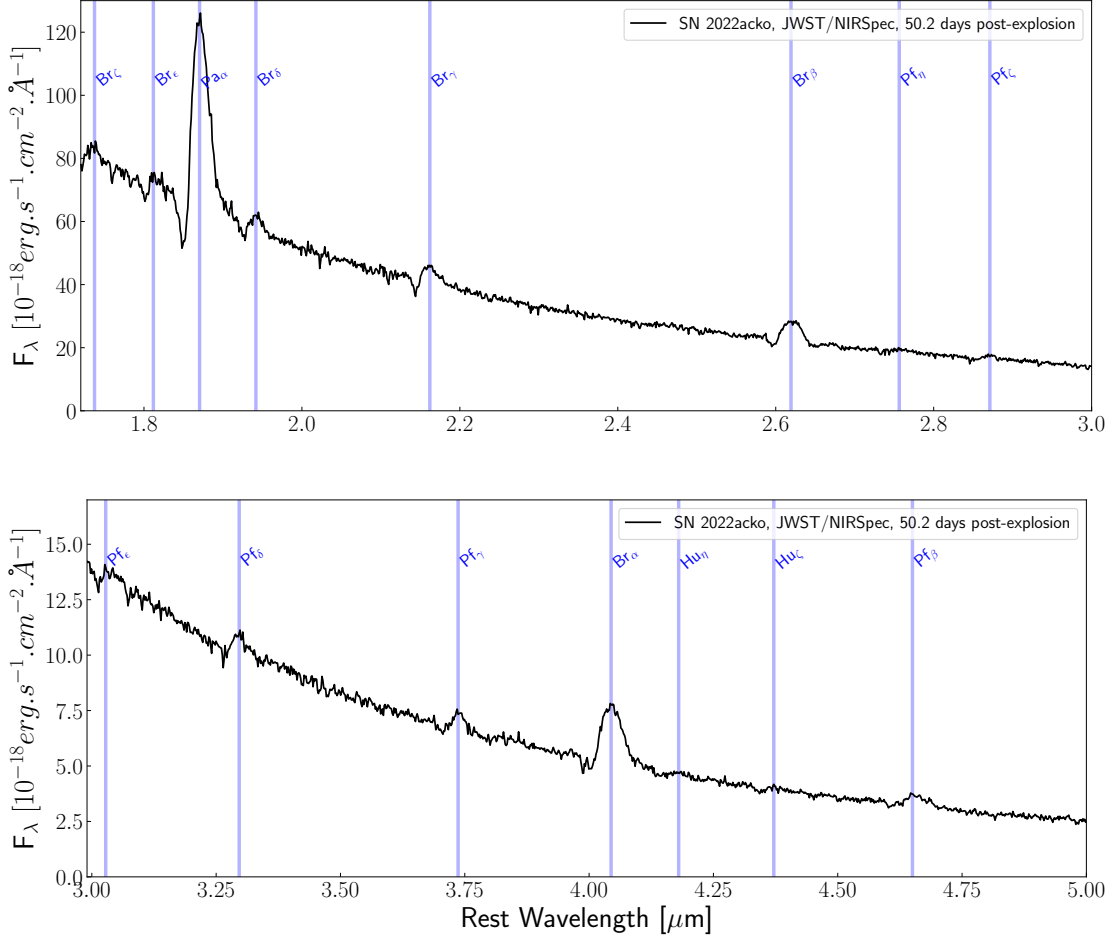


Figure 5. *First:* The JWST-NIRSpec S400A1/F170P spectrum with labeled line IDs. *Second:* The JWST-NIRSpec S400A1/F290P spectrum with labeled line IDs.

fit with a blackbody function, the SED produces a temperature of ~ 4000 K.

We compared the *JWST* photometry with SN 2022acko’s SED and found the NIRspec and MIRI spectra to be consistent with the photometry, except for wavelengths longer than $18 \mu\text{m}$, where the MIRI spectrum increases in flux. The background in Channel 4 causes this increase in the spectral flux and is not intrinsic to the SNe or environment. Hence, we see no evidence of pre-existing dust or molecules in the SN 2022acko, and this statement will be quantified below.

6. LIMITS ON CO FORMATION AND PRE-EXISTING MOLECULES AND DUST

To obtain upper limits on the *CO* formation, we use our framework MOLFIT which provides an interactive layer based on the module for calculating the vibrational and rotational bands of molecules and for spherical radiation transport in HYDRA (see (Sharp & Höflich 1989; Höflich 1988; Gérard et al. 2000; Höflich et al. 2002; Rho et al. 2021), and references therein). To reproduce the observations the

following free parameters are used: a) temperature, b) density represented by a power law $\propto \rho^n$, c) abundances, d) small-scale random motion such as turbulent motion v_{turb} , e) average expansion velocity v of a shell of thickness δv , and f) the *CO*⁺/*CO* ratio to mimic the possible exposure to hard γ -rays. Rather than solving the time-dependent rate equations for molecule formation and radiation transport in HYDRA, local-thermodynamical equilibrium is used for the molecule to atomic abundances. Note that the *CO* concentration in LTE is an upper limit for a rapidly expanding atmospheres because the formation times scale for *CO* are comparable to geometrical dilution by expansion, with an additional role of hard radiation as discussed (see, for example Rho et al. 2021). It is well known that for the formation and destruction, time-dependent rate equations for $C + O \rightarrow CO$, $C^+ + O \rightarrow CO^+$ are needed. The exposure of the ejecta to γ -rays by ⁵⁶Ni mixing may increase the *CO* formation unless the resulting destruction outweighs the formation rate via the $C + O^+ \rightarrow CO^+$ channel, and that the thermodynamic equilibrium abundance is larger than the *CO* abundances obtained by the time-dependent rate

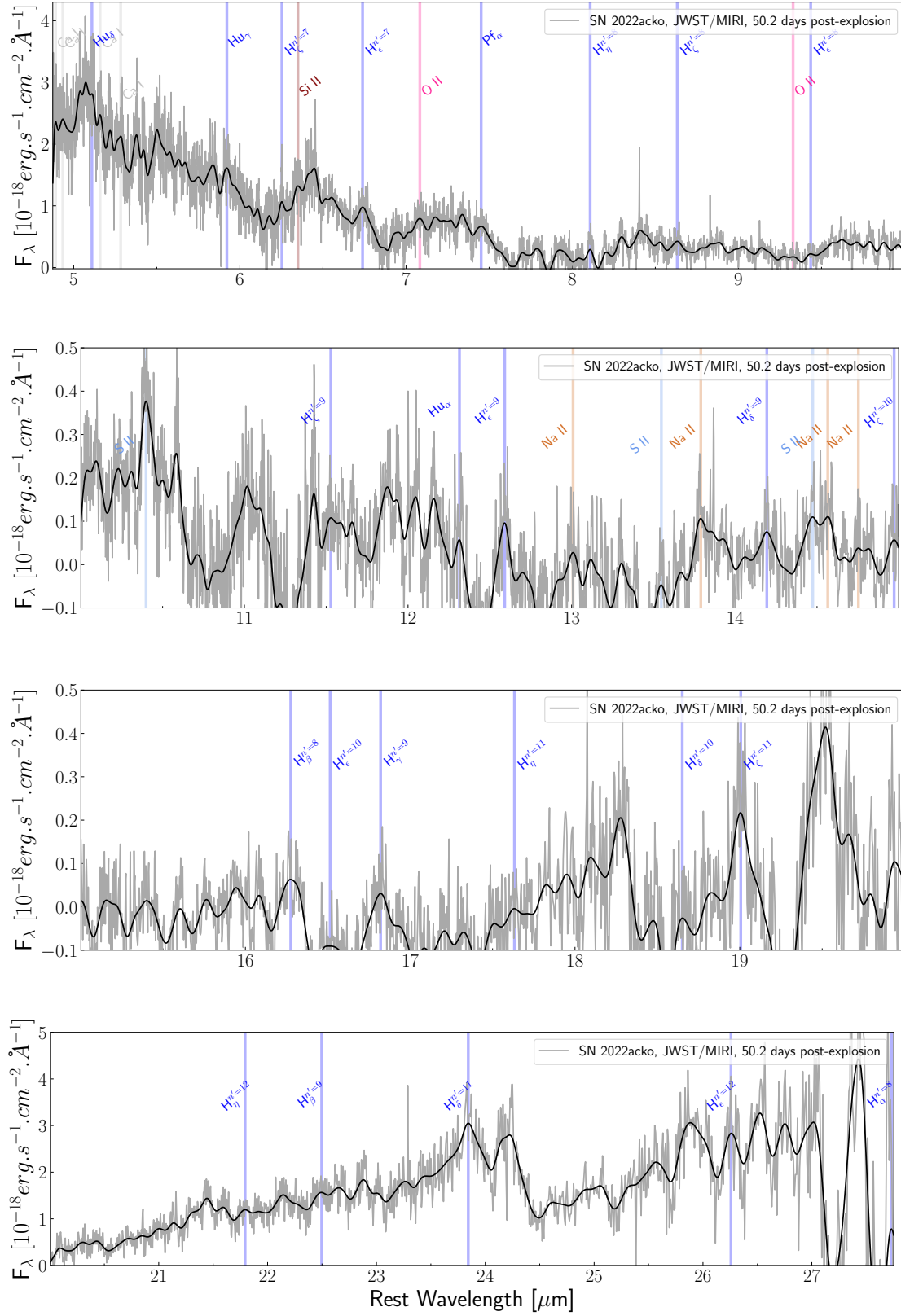


Figure 6. The reduced stitch 4 channel MIRI-MRS spectrum of SN 2022acko with line identifications. Line identifications in Channel 4 are tentative due to the large background on the observations.

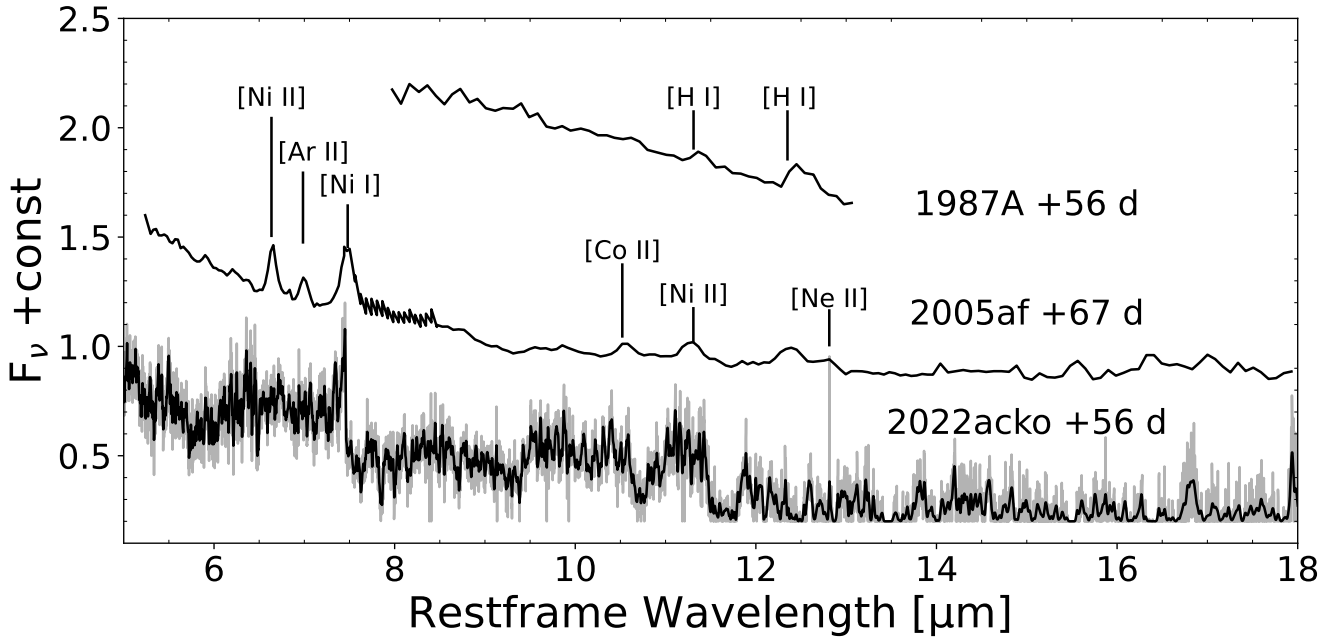


Figure 7. Comparison between MIR spectra of SN 1987A, 2005af and 2022acko. the forbidden lines seen in the day 67 spectrum of SN 2005af are absent in earlier spectra of SN 1987A and 2022acko. This is because at these phases SN 2005af was at the end of the plateau. the data from SN 1987A are digitalized from Aitken et al. (1988); Bouchet et al. (1989).

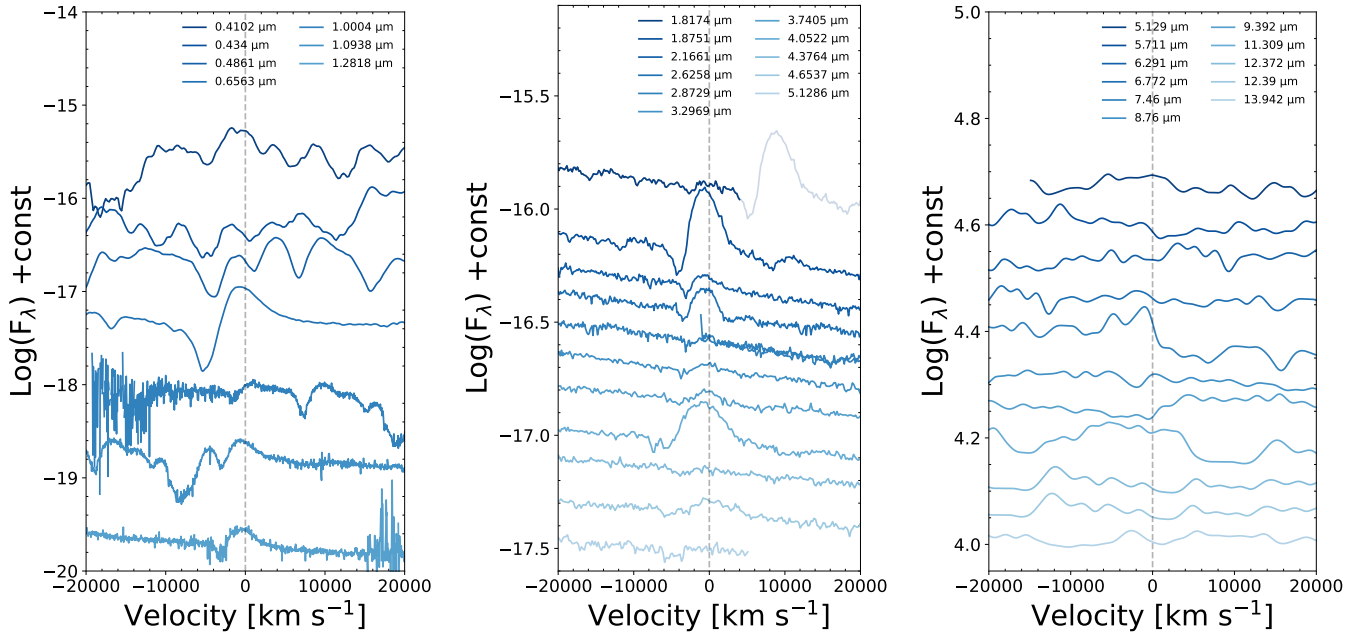


Figure 8. The H line velocity profiles from the optical to the MIR wavelengths. We identify 29 potential H features in the ground-based optical and NIR spectra (left), the JWST NIR spectra (middle), and the JWST mid-IR spectra (Right).

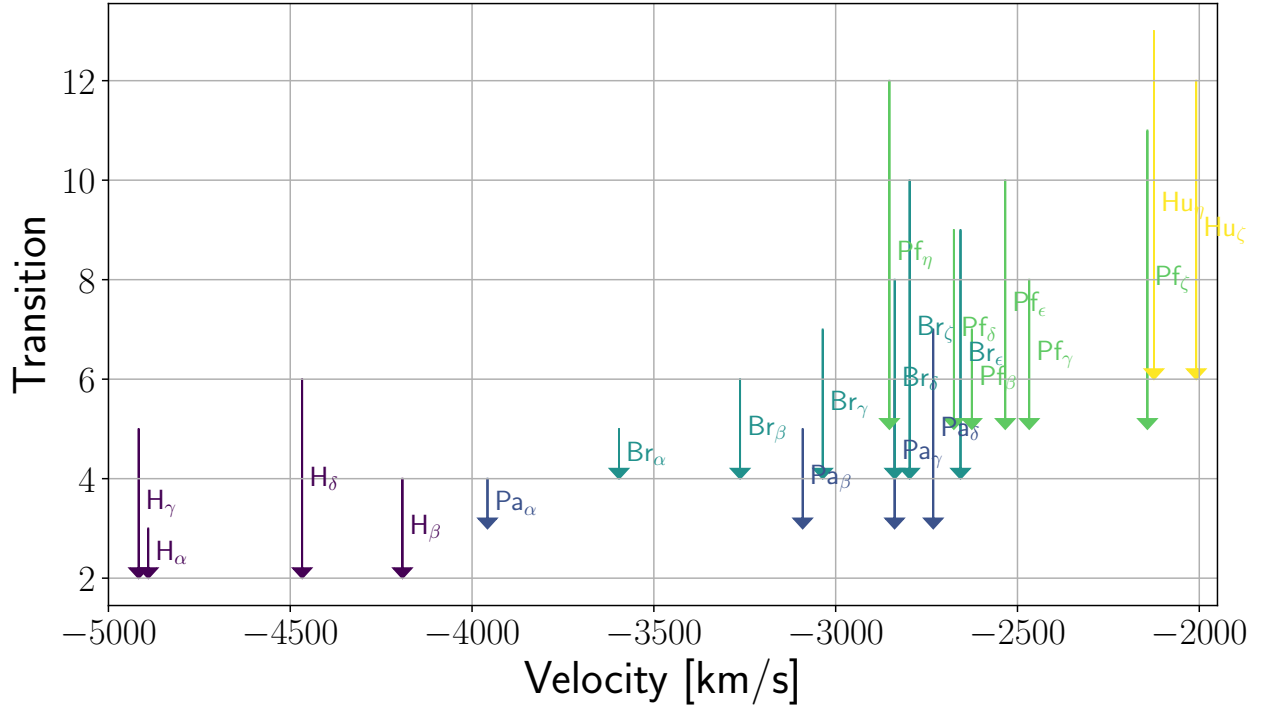


Figure 9. The minimum velocity of each hydrogen feature against the transition at which it occurs.

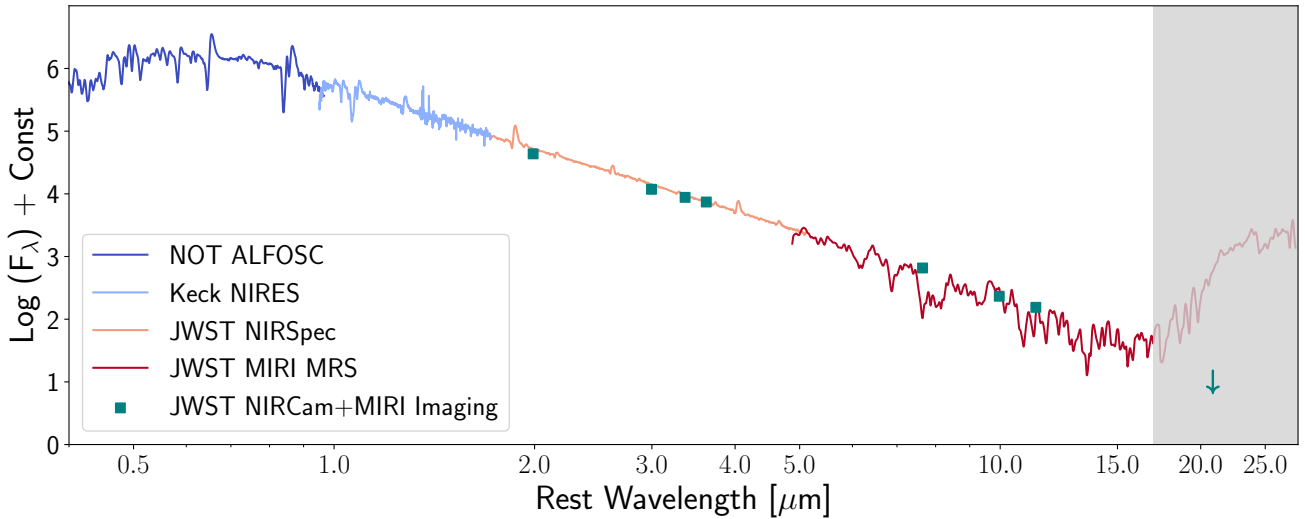


Figure 10. The spectral energy distribution of SN 2022acko extending between 0.4–25 μm . A constant has shifted the Keck (+ NIRES) spectrum to match the optical NOT (+ ALFOSC) and the *JWST* spectra. The NIRSpec and MIRI fluxing is consistent with the multi-band *JWST* photometry, except in Channel 4, where the background dominates the spectral flux. The F_{2100W} -band photometry sets an important base level for future *JWST* observations. SN 2022acko fit with a blackbody function characterized by $T_{eff} = 4000 \text{ K} \pm 500$ is shown in golden.

Table 4. SN 2022acko spectral lines.

Ion	Wavelength [μm]	Ion	Wavelength [μm]	Ion	Wavelength [μm]
Optical spectrum					
H I	0.4861	Sc III	0.6238	Sc III	0.7449
H I	0.3889	H I	0.6563	H I	0.9229
Ca II	0.3969	Fe II	0.4924	Ca II	0.8498
H I	0.3970	Fe II	0.5169	Ca II	0.8498
Ca II	0.3934	Sc II	0.5527	Ca II	0.8542
H I	0.4102	Sc II	0.5698	Ca II	0.8662
H I	0.4341	O I	0.7774	Mg II	0.9218
Fe II	0.4358	Na I	0.5894	C I	0.9408
Fe II	0.4642	Ba II	0.6142	H I	0.9014
Ground-based NIR spectrum					
H I	1.005	Mg II	1.0092	O I	1.1290
H I	1.0938	Mg II	1.0927	Sr II	1.0330
H I	1.2818	Na I	1.0749	Sr II	1.0920
Ca II	1.1839	C I	1.1333		
Ca II	1.1950	C I	1.1756		
NIRSpec spectrum					
H I	1.817	H I	2.626	H I	4.052
H I	1.875	H I	2.873	H I	4.377
H I	1.944	H I	3.297	H I	4.654
H I	2.166	H I	3.741	H I	5.129
MIRI/MRS spectrum					
H I	5.129	O I	10.384	Fe I	16.596
C II	5.539	O I	10.399	H I	16.881
H I	5.711	H I	11.309	H I	18.615
C II	5.836	O I	11.853	N I	18.811
H I	6.291	O I	12.058	H I	18.978
H I	6.772	H I	12.372	H I	19.062
C II	6.775	H I	12.390	N I	19.616
C II	6.900	O I	12.995	N I	19.641
H I	7.460	C I	13.297	N I	20.353
O I	7.720	C I	13.370	N I	21.022
C I	8.374	C I	13.872	C I	22.278
N II	8.439	H I	13.942	H I	23.868
H I	8.760	H I	14.183	N I	25.058
N III	9.175	H I	14.962	H I	26.168
N III	9.191	Fe I	15.561	H I	26.682
O II	9.332	C I	15.803	C I	27.425
H I	9.392	Fe I	16.107	H I	27.803
O II	9.439	H I	16.209		

Table 5. H I absorption velocities. Spectral lines affected by significant blending are indicated with an *.

Species	Rest Wavelength [μm]	Velocity [km s^{-1}]	Error [km s^{-1}]
H γ	0.434	-4900	900
H β	0.486	-4200	900
H α	0.656	-4900	900
Pa η *	0.901	400	900
Pa ζ *	0.923	-2300	900
Pa ϵ *	0.955	-2400	900
Pa δ	1.005	-2700	200
Pa γ	1.094	-2800	100
Pa β	1.282	-3100	100
Pa α	1.876	-4000	300
Br ζ	1.737	-2800	400
Br ϵ	1.818	-2700	400
Br δ	1.945	-2800	400
Br γ	2.166	-3000	300
Br β	2.626	-3300	300
Pf η	2.758	-2900	300
Pf ζ	2.873	-2100	400
Pf ϵ	3.039	-2500	300
Pf δ	3.297	-2700	400
Pf γ	3.741	-2500	400
Br α	4.052	-3600	400
Hu η	4.171	-2100	400
Hu ζ	4.376	-2000	400
Pf β	4.654	-2600	400

equations (Spyromilio et al. 1988; Sharp & Hoefflich 1990; Lepp et al. 1990; Meikle et al. 1993; Rho et al. 2019). Time-dependent rate equation effects have been included in models for SN 1987A and stripped-envelope SNe (Sharp & Höflich 1989; Sharp & Hoefflich 1990; Gerardy et al. 2000). Including these effects would result in a smaller upper limit of the CO-mass given below. For the simulations, 50,000 to 300,000 vibrational transitions have been taken into account for each CO, CO⁺ and SiO.

6.1. CO formation in the SN-ejecta

The spectrum of SN 2022acko does not show evidence for the formation of molecules. However, our data provides important upper limits on the amount of pre-existing molecules and dust, which is required to set a baseline for observations at later times. In addition, it probes the mixing of C/O rich material into the H-rich envelope. It is well-established for CCSNe with a massive H-rich envelope, that molecule formation starts when the C/O core gets exposed or when C/O plumes are mixed into the H-rich envelope through rayleigh

taylor instabilities. This also only occurs when the temperature drops below $T \approx 5000$ K (Liu & Dalgarno 1995; Gerardy et al. 2000). For example, in SN 1987A, there was observational evidence for mixing of C/O up to $v \approx 3000$ km s⁻¹ and H-rich material down to $v \approx 800$ km s⁻¹ (Larson et al. 1987; Catchpole et al. 1987; Hoefflich 1988). Mixing has been discussed for other SNe II (Gerardy et al. 2000; Kotak et al. 2005b; Meikle et al. 2007b; Kotak et al. 2009; Rho et al. 2018; Davis et al. 2019). This mixing of C/O rich material was understood as due to Rayleigh-Taylor instabilities developing in the ejecta between different chemical layers (Muller et al. 1989; Fryxell et al. 1991; Nagataki et al. 1998).

For SN 2022acko, to obtain upper limits for CO during the plateau phase, we assumed a density structure and temperatures, T , typical for a SN IIP that has an effective temperature $T \approx 5500$ K and a rapid drop in T well below 5000 K to about 2500–4000 K as the photosphere recedes (Turatto et al. 1993; Chieffi et al. 2003; Dessart et al. 2013). For a specific example, see Figs. 12–13 in Chieffi et al. (2003). For the density gradient, we use the ratio of hydrogen absorption line shifts within each series of H-line features which is limited by the optical depth of 1 in the line where each member of a series has the same lower level or the optical depth of 1 in Thomson scattering, as previously employed for e.g. SN 1987A (Hoefflich 1988), and SN 1998S (Gerardy et al. 2002). Comparing the velocities obtained for transitions with the same lower level from Table 5 and Fig. 9 and assuming this corresponds to the point where $\tau = 1$ for this transition, we obtain $2.1 < n < 2.6$ assuming the density follows a powerlaw, $\rho \propto r^{-n}$ (Hoefflich 1990; Duschinger et al. 1995).

During the plateau, the location of the photosphere is determined by the recombination of H, because the opacities drop by 2 to 4 orders of magnitude (see, for example Chieffi et al. 2003, their Figure 13).

Fig. 11 shows the scaled opacity (top) for both the fundamental (right) and first overtone (left) of CO, and their flux for given temperatures comparison with observation (bottom). The opacity peaks at about 2500–3000 K and decreases by about six orders of magnitude towards the recombination temperature of H. For lower temperatures, the flux in the fundamental band scales $\propto T$ as expected, whereas the first overtone flux drops explaining why this band vanishes at about day 200 in SNe IIP (Gerardy et al. 2000). Because the opacity and the specific emissivity relative to the continuum flux in the first CO overtone is smaller than the fundamental band by a factor on the order of $\approx 10^2$, the fundamental band provides the upper limits, showing the importance of JWST data.

At the inner edge of the photosphere ($T \approx 5000 - 5500$ K), when compared to an outer region ($T \sim 4000$ K), the CO opacity is reduced by factors of three to four orders of magnitude, thus providing a sharp inner boundary for the CO emission. For $T = 4000$ K, we obtain $M(\text{CO}) \approx 2 \times 10^{-6} M_{\odot}$

(Fig. 11, lower right), under the reasonable assumption that the mixing of C/O rich material does not stop exactly at the photosphere. We have divided our upper limit by the signal to noise ratio (S/N ≈ 44) To obtain an upper limit for CO, we assume the potential CO feature to be optically thin with an amplitude less than the S/N of the observed spectrum.

7. COMPARISON TO SN 1987A AND LIMITS ON MIXING DURING THE EXPLOSION

In SN 2022acko, the C/O-rich layers are not mixed into the H-rich layers expanding with $\approx 2000 - 2500$ km s⁻¹ as in SN 1987A. At the epoch with similar expansion at the photosphere and light curve phase determined by the H-recombination, SN 1987A showed extended mixing of H down to 800 km s⁻¹ and CO out to 3000 km s⁻¹ (Danziger 1988; Hoefflich 1988; Meikle 1988), whereas SN 2022acko shows no evidence for any mixing during the explosion.

From Table 5 we see that the hydrogen lines in SN 2022acko are in a velocity range from $\sim 2000 - 5000$ km s⁻¹. The line profiles in the infrared exhibit the traditional P Cygni shape. In the case of SN 1987A the profiles, while still generally P Cygni, showed a double-peaked emission which is very apparent in Pa_{α} as well as the Balmer lines (Larson et al. 1987; Catchpole et al. 1987). This was interpreted to be caused by mixing of C/O into the H-rich envelope as well as of H into the C/O core (Hoefflich 1988). This would be from Rayleigh Taylor instabilities caused by the shock propagation through the ejecta prior to the onset of homology (Muller et al. 1989; Fryxell et al. 1991; Nagataki et al. 1998). Given the lack of evidence for asymmetry in the H lines, as well as a lack of CO formation, we conclude that mixing in SN 2022acko is significantly below that of SN 1987A, likely due to the the difference in progenitor history. Hence, any freshly formed CO observable at later times in SN 2022acko should be attributed to CO formation in the C/O core.

7.1. Molecules in the Circumstellar Material

If CO exists in the CSM it would add opacity due to cold CO in the surroundings of SN 2022acko. Since we do not see CO, any pre-existing CO is optically thin. The emission will be $\propto T$ in the fundamental band with most of the power emitted in the first overtone of the fundamental band. Using the scaling in Fig. 11, the upper limits of $M(\text{CO})$ in the CSM at $T = 1000, 500,$ and 100 K are $10^{-8}, 2 \times 10^{-8}$ and $10^{-7} M_{\odot}$, respectively. If CO is observed in SN 2022acko at later times, it will be due to freshly synthesized molecules.

7.2. Pre-existing dust in the Interstellar and Circumstellar Medium

In principle, an upper limit for dust in the ISM and CSM can be obtained the same way as for CO above. However, the absorption to emission ratio depends sensitively upon the

grain-size distribution. For spherical dust, the surface to mass ratio $\propto 1/R$ where R is the dust radius for particles larger than the wavelength of light or is given by Rayleigh scattering for shorter wavelengths. In the absence of observed dust signatures, we conclude that there is no evidence for ISM or CSM dust or a warm dust component.

8. CONCLUSIONS

In this work, we presented the first *JWST* spectrum of a CCSN, 2022acko. The data were obtained ~ 52 days after the explosion epoch, overlapping with the H-recombination phase. Hydrogen lines mainly dominate the spectra of SN 2022acko but also contain spectral lines from C, N, Na, O, Mg, Br, Sc, and Fe. Combining our *JWST* data with ground-based optical and NIR spectra, we created a full SED ranging from 0.4-25 μm . The spectrum of SN 2022acko is found to resemble similar epoch spectra of SN 1987A and SN 2005af. However, by these phases, SN 2005af already showed forbidden lines while SN 2022acko does not. This may suggest that SN 2022acko is evolving more slowly than SN 2005af. One should note that the exact phase of SN 2005af is rather uncertain.

We have shown that the *JWST* spectra provide new constraints on the underlying physics of SNe IIP. Our analysis of the multi-wavelength spectra allows us to identify lines of carbon, nitrogen, and oxygen as well as s-process elements, which confirms the expected evolutionary phases of a pre-SN red supergiant including AGB-like burning conditions occurring in the ejecta leading to s-process production.

We also demonstrate that placing limits on the flux level of the fundamental band of *CO* can be used to measure the processes happening during the stellar evolution, the explosion, and within the environment. We see no extended mixing of the H and the C/O core is present at this epoch, and place tight upper limits on the *CO* mass. We can rule out significant mixing via Raleigh Taylor instabilities in the ejecta or a heavily asymmetric explosion. Finally, we demonstrate that *JWST* is needed for finding the pre-existing *CO* mass, and conclude that SN 2022acko has no detectable, pre-existing *CO* ($< 10^{-8} M_{\odot}$), as well as no dust in the CSM. This important finding provides a clean slate for future *JWST* observations which will probe molecule and dust formation in SN 2022acko at later times. Any molecules or dust seen in future *JWST* epochs will be newly formed, since this epoch has served to rule out the presence of any pre-existing dust or molecules.

The observations from this work set a critical baseline for molecule and dust formation in SN 2022acko. Future *JWST* spectroscopic observations of SN 2022acko will provide important information on the formation of *CO*, *SiO*, and dust. Comparison of the rate of molecule and dust formation with SNe 1987A, 2004dj, and 2005af will provide important clues into the dust budget of SNe IIP in general as well as the variation within the SNe IIP subclass.

We thank Jozsef Vinko for providing us with electronic versions of Spitzer spectra. MS acknowledges support by NASA grant JWST-GO-04436, JWST-GO-04217, JWST-GO-01860, JWST-GO-02666. This work was supported by a NASA Keck PI Data Award, administered by the NASA Exoplanet Science Institute. The Observatory was made possible by the generous financial support of the W. M. Keck Foundation. The authors wish to recognize and acknowledge the very significant cultural role and reverence that the summit of Maunakea has always had within the indigenous Hawaiian community. We are most fortunate to have the opportunity to conduct observations from this mountain. CA, PH, EB, and JD acknowledge support by NASA grant JWST-GO-02114, JWST-GO-02122, JWST-GO-04436, and JWST-GO-04522. Support for program #2122 was provided by NASA through a grant from the Space Telescope Science Institute, which is operated by the Association of Universities for Research in Astronomy, Inc., under NASA contract NAS 5-03127. PH acknowledges support by the National Science Foundation (NSF) through grant AST-2306395 and NASA grant 80NSSC20K0538. EB acknowledges support by NASA grant 80NSSC20K0538. MDS is funded by the Independent Research Fund Denmark (IRFD, grant number 10.46540/2032-00022B). This publication was made possible through the support of an LSSTC Catalyst Fellowship to KAB funded through Grant 62192 from the John Templeton Foundation to LSST Corporation. The opinions expressed in this publication are those of the author(s) and do not necessarily reflect the views of LSSTC or the John Templeton Foundation. ID acknowledges partial support by the Spanish project PID2021-123110NB 100 financed by MCIN/AEI/10.13039/501100011033/FEDER/UE. LG acknowledges financial support from the Spanish Ministerio de Ciencia e Innovación (MCIN), the Agencia Estatal de Investigación (AEI) 10.13039/501100011033, and the European Social Fund (ESF) "Investing in your future" under the 2019 Ramón y Cajal program RYC2019-027683-I and the PID2020-115253GA-I00 HOSTFLOWS project, from Centro Superior de Investigaciones Científicas (CSIC) under the PIE project 20215AT016, and the program Unidad de Excelencia María de Maeztu CEX2020-001058-M. The research of YY is supported through a Bengier-Winslow-Robertson Fellowship. SM acknowledges support from the Magnus Ehrnrooth Foundation and the Vilho, Yrjö and Kalle Väisälä Foundation. This work is based on observations made with the NASA/ESA/CSA James Webb Space Telescope. The data were obtained from the Mikulski Archive for Space Telescopes at the Space Telescope Science Institute, which is operated by the Association of Universities for Research in Astronomy, Inc., under NASA contract NAS 5-03127 for *JWST*. These observations are associated with program #2122.

We acknowledge the Keck Infrared Transient Survey (KITS), which was executed primarily by members of the UC Santa Cruz transients team, who were supported in part by NASA grants NNG17PX03C, 80NSSC21K2076z, 80NSSC22K1513, 80NSSC22K1518; NSF grant AST-1911206; and by fellowships from the Alfred P. Sloan Foundation and the David and Lucile Packard Found-

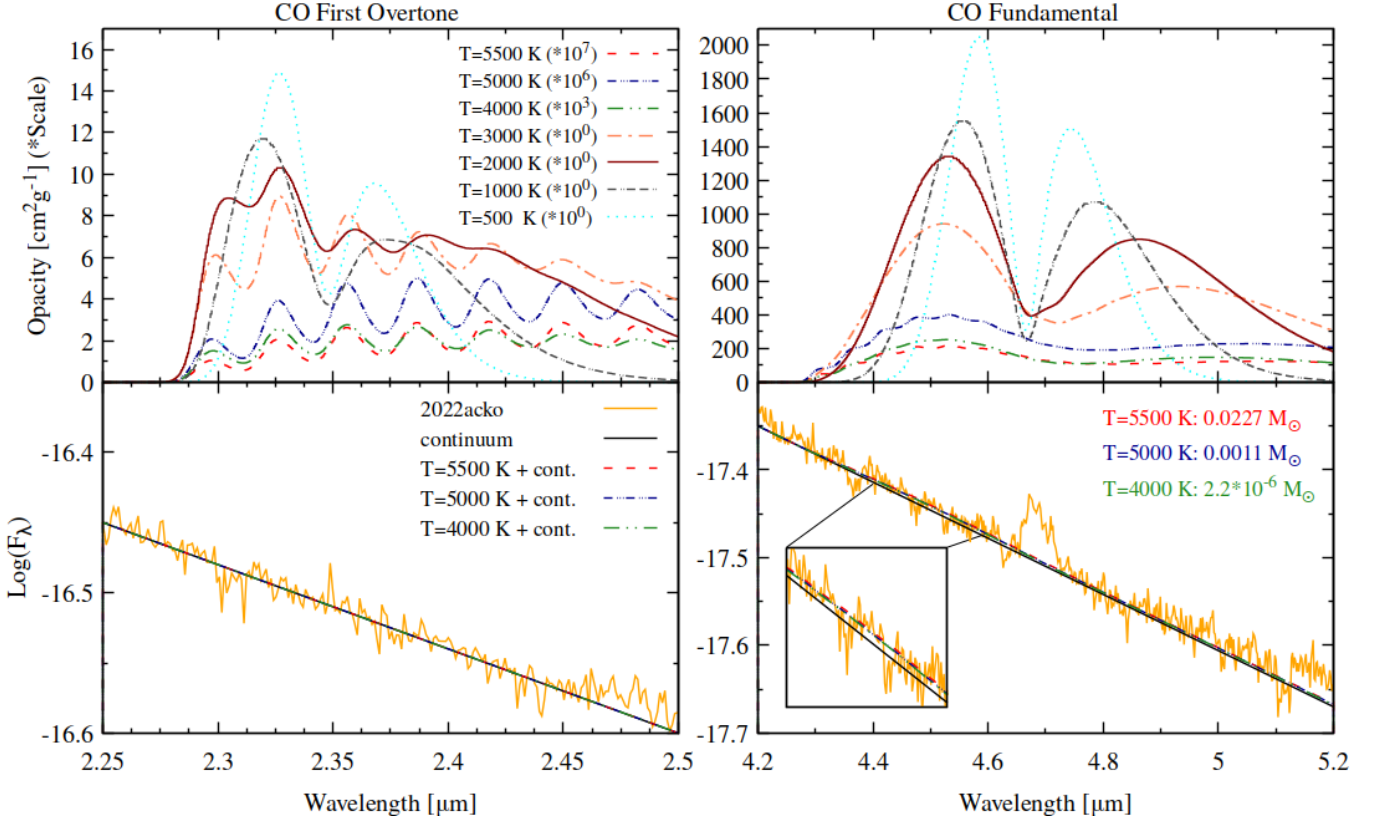


Figure 11. Limits of CO in SN 2022acko. CO opacities $\text{cm}^2 \text{g}^{-1} \text{ \AA}$ with scale factors of the 1^{st} (upper left) and fundamental band (upper right) of CO , and the comparison of the continuum + CO emission and observation with the total CO masses based on the fundamental band. The specific CO -emissivity is given by the product of opacity and black body. For the upper limit of the CO emission, we assumed the S/N as limit for the relative flux contribution. The underlying continuum the CO feature is approximated akin a Blackbody. The upwards slope beyond $4.8 \mu\text{m}$ hints that free-free emission is present. Note that the mass limits based on the 1^{st} CO would be larger by a factor of ≈ 100 , clearly demonstrating the need for *JWST* observations.

Facilities: *JWST* (MRS/MIRI,NIRSpec/MIRI), MAST (*JWST*)

Software: *jwst* (ver. 1.9.4, Bushouse et al. 2023), *jdaviz* (ver. 3.2.1, Developers et al. 2023), *HYDRA* (Höflich 2003, 2009; Höflich et al. 2017), *OpenDx* (an open-sourced visualization package developed by IBM), *Astropy* (Astropy Collaboration et al. 2013, 2018, 2022), *NumPy* (Harris et al. 2020), *SciPy* (Virtanen et al. 2020), *Matplotlib* (Hunter 2007), *pypeit* (Prochaska et al. 2020).

REFERENCES

- Aitken, D. K., Smith, C. H., James, S. D., et al. 1988, *MNRAS*, 235, 19P, doi: [10.1093/mnras/235.1.19P](https://doi.org/10.1093/mnras/235.1.19P)
- Anand, G. S., Lee, J. C., Van Dyk, S. D., et al. 2021, *MNRAS*, 501, 3621, doi: [10.1093/mnras/staa3668](https://doi.org/10.1093/mnras/staa3668)
- Astropy Collaboration, Robitaille, T. P., Tollerud, E. J., et al. 2013, *A&A*, 558, A33, doi: [10.1051/0004-6361/201322068](https://doi.org/10.1051/0004-6361/201322068)
- Astropy Collaboration, Price-Whelan, A. M., Sipőcz, B. M., et al. 2018, *AJ*, 156, 123, doi: [10.3847/1538-3881/aabc4f](https://doi.org/10.3847/1538-3881/aabc4f)
- Astropy Collaboration, Price-Whelan, A. M., Lim, P. L., et al. 2022, *apj*, 935, 167, doi: [10.3847/1538-4357/ac7c74](https://doi.org/10.3847/1538-4357/ac7c74)
- Baron, E., Nugent, P. E., Branch, D., et al. 2003, *ApJ*, 586, 1199, doi: [10.1086/367888](https://doi.org/10.1086/367888)
- Bertoldi, F., Cox, P., Neri, R., et al. 2003, *A&A*, 409, L47, doi: [10.1051/0004-6361:20031345](https://doi.org/10.1051/0004-6361:20031345)
- Bostroem, K. A., Dessart, L., Hillier, D. J., et al. 2023, *ApJL*, 953, L18, doi: [10.3847/2041-8213/ace31c](https://doi.org/10.3847/2041-8213/ace31c)
- Bouchet, P., Moneti, A., Slezak, E., Le Bertre, T., & Manfroid, J. 1989, *A&AS*, 80, 379
- Bouchet, P., García-Marín, M., Lagage, P. O., et al. 2015, *PASP*, 127, 612, doi: [10.1086/682254](https://doi.org/10.1086/682254)
- Bushouse, H., Eisenhamer, J., Dencheva, N., et al. 2023, *JWST Calibration Pipeline*, 1.9.4, Zenodo, doi: [10.5281/zenodo.7577320](https://doi.org/10.5281/zenodo.7577320)
- Catchpole, R. M., Menzies, J. W., Monk, A. S., et al. 1987, *MNRAS*, 229, 15P, doi: [10.1093/mnras/229.1.15P](https://doi.org/10.1093/mnras/229.1.15P)
- Catchpole, R. M., Whitelock, P. A., Feast, M. W., et al. 1988, *MNRAS*, 231, 75P, doi: [10.1093/mnras/231.1.75P](https://doi.org/10.1093/mnras/231.1.75P)
- Cernuschi, F., Marsicano, F., & Codina, S. 1967, *Annales d'Astrophysique*, 30, 1039
- Cherchneff, I., & Dwek, E. 2009, *ApJ*, 703, 642, doi: [10.1088/0004-637X/703/1/642](https://doi.org/10.1088/0004-637X/703/1/642)
- Chieffi, A., Domínguez, I., Höflich, P., Limongi, M., & Straniero, O. 2003, *MNRAS*, 345, 111, doi: [10.1046/j.1365-8711.2003.06958.x](https://doi.org/10.1046/j.1365-8711.2003.06958.x)
- Danziger, I. J. 1988, in *Origin and Distribution of the Elements*, ed. G. J. Mathews, 407
- Davis, S., Hsiao, E. Y., Ashall, C., et al. 2019, *ApJ*, 887, 4, doi: [10.3847/1538-4357/ab4c40](https://doi.org/10.3847/1538-4357/ab4c40)
- de Vaucouleurs, G., de Vaucouleurs, A., Corwin, Herold G., J., et al. 1991, *Third Reference Catalogue of Bright Galaxies*
- Dessart, L., Hillier, D. J., Waldman, R., & Livne, E. 2013, *MNRAS*, 433, 1745, doi: [10.1093/mnras/stt861](https://doi.org/10.1093/mnras/stt861)
- Developers, J., Averbukh, J., Bradley, L., et al. 2023, *Jdaviz*, 3.2.1, Zenodo, doi: [10.5281/zenodo.7600492](https://doi.org/10.5281/zenodo.7600492)
- Duschinger, M., Puls, J., Branch, D., Höflich, P., & Gabler, A. 1995, *A&A*, 297, 802
- Dwek, E., Galliano, F., & Jones, A. P. 2007, *ApJ*, 662, 927, doi: [10.1086/518430](https://doi.org/10.1086/518430)
- Ferrarotti, A. S., & Gail, H. P. 2006, *A&A*, 447, 553, doi: [10.1051/0004-6361:20041198](https://doi.org/10.1051/0004-6361:20041198)
- Fox, O. D., Chevalier, R. A., Dwek, E., et al. 2010, *ApJ*, 725, 1768, doi: [10.1088/0004-637X/725/2/1768](https://doi.org/10.1088/0004-637X/725/2/1768)
- Fryxell, B., Mueller, E., & Arnett, D. 1991, *ApJ*, 367, 619, doi: [10.1086/169657](https://doi.org/10.1086/169657)
- Gall, C., Hjorth, J., & Andersen, A. C. 2011, *A&A Rv*, 19, 43, doi: [10.1007/s00159-011-0043-7](https://doi.org/10.1007/s00159-011-0043-7)
- Gérard, J.-C., Hubert, B., Bisikalo, D. V., & Shematovich, V. I. 2000, *J. Geophys. Res.*, 105, 15795, doi: [10.1029/1999JA002002](https://doi.org/10.1029/1999JA002002)
- Gerardy, C. L., Fesen, R. A., Höflich, P., & Wheeler, J. C. 2000, *AJ*, 119, 2968, doi: [10.1086/301390](https://doi.org/10.1086/301390)
- Gerardy, C. L., Fesen, R. A., Nomoto, K., et al. 2002, *PASJ*, 54, 905, doi: [10.1093/pasj/54.6.905](https://doi.org/10.1093/pasj/54.6.905)
- González Delgado, D., Olofsson, H., Kerschbaum, F., et al. 2003, *A&A*, 411, 123, doi: [10.1051/0004-6361:20031068](https://doi.org/10.1051/0004-6361:20031068)
- Harris, C. R., Millman, K. J., van der Walt, S. J., et al. 2020, *Nature*, 585, 357, doi: [10.1038/s41586-020-2649-2](https://doi.org/10.1038/s41586-020-2649-2)
- Höflich, P. 1988, *PASA*, 7, 434, doi: [10.1017/S1323358000022608](https://doi.org/10.1017/S1323358000022608)
- Höflich, P., Hsiao, E. Y., Ashall, C., et al. 2017, *ApJ*, 846, 58, doi: [10.3847/1538-4357/aa84b2](https://doi.org/10.3847/1538-4357/aa84b2)
- Höflich, P. 1990, PhD thesis, -
- Höflich, P. 2003, in *Astronomical Society of the Pacific Conference Series*, Vol. 288, *Stellar Atmosphere Modeling*, ed. I. Hubeny, D. Mihalas, & K. Werner, 185
- Höflich, P. 2009, in *American Institute of Physics Conference Series*, Vol. 1171, *Recent Directions in Astrophysical Quantitative Spectroscopy and Radiation Hydrodynamics*, ed. I. Hubeny, J. M. Stone, K. MacGregor, & K. Werner, 161–172, doi: [10.1063/1.3250057](https://doi.org/10.1063/1.3250057)
- Höflich, P., Gerardy, C. L., Fesen, R. A., & Sakai, S. 2002, *ApJ*, 568, 791, doi: [10.1086/339063](https://doi.org/10.1086/339063)
- Hoyle, F., & Wickramasinghe, N. C. 1970, *Nature*, 226, 62, doi: [10.1038/226062a0](https://doi.org/10.1038/226062a0)
- Hunter, J. D. 2007, *Computing in Science and Engineering*, 9, 90, doi: [10.1109/MCSE.2007.55](https://doi.org/10.1109/MCSE.2007.55)
- Jakobsen, P., Ferruit, P., Alves de Oliveira, C., et al. 2022, *A&A*, 661, A80, doi: [10.1051/0004-6361/202142663](https://doi.org/10.1051/0004-6361/202142663)
- Kotak, R., Meikle, P., van Dyk, S. D., Höflich, P. A., & Mattila, S. 2005a, *ApJL*, 628, L123, doi: [10.1086/432719](https://doi.org/10.1086/432719)
- . 2005b, *ApJL*, 628, L123, doi: [10.1086/432719](https://doi.org/10.1086/432719)
- Kotak, R., Meikle, P., Pozzo, M., et al. 2006, *ApJL*, 651, L117, doi: [10.1086/509655](https://doi.org/10.1086/509655)
- Kotak, R., Meikle, W. P. S., Farrah, D., et al. 2009, *ApJ*, 704, 306, doi: [10.1088/0004-637X/704/1/306](https://doi.org/10.1088/0004-637X/704/1/306)

- Larson, H. P., Drapatz, S., Mumma, M. J., & Weaver, H. A. 1987, in *European Southern Observatory Conference and Workshop Proceedings*, Vol. 26, European Southern Observatory Conference and Workshop Proceedings, 147
- Lee, J. C., Sandstrom, K. M., Leroy, A. K., et al. 2023, *ApJL*, 944, L17, doi: [10.3847/2041-8213/acaaae](https://doi.org/10.3847/2041-8213/acaaae)
- Lepp, S., Dalgarno, A., & McCray, R. 1990, *ApJ*, 358, 262, doi: [10.1086/168981](https://doi.org/10.1086/168981)
- Li, L., Cai, Y., Zhai, Q., Zhang, J., & Wang, X. 2022, *Transient Name Server Classification Report*, 2022-3549, 1
- Li, Q., Wang, R., Fan, X., et al. 2020, *ApJ*, 900, 12, doi: [10.3847/1538-4357/aba52d](https://doi.org/10.3847/1538-4357/aba52d)
- Liu, W., & Dalgarno, A. 1995, *ApJ*, 454, 472, doi: [10.1086/176498](https://doi.org/10.1086/176498)
- Lundquist, M., Pearson, J., Paraskeva, E., et al. 2022, *Transient Name Server Discovery Report*, 2022-3543, 1
- Maiolino, R., Schneider, R., Oliva, E., et al. 2004, *Nature*, 431, 533, doi: [10.1038/nature02930](https://doi.org/10.1038/nature02930)
- Mazzali, P. A., Lucy, L. B., & Butler, K. 1992, *A&A*, 258, 399
- Meikle, W. P. S. 1988, *PASA*, 7, 473, doi: [10.1017/S1323358000022669](https://doi.org/10.1017/S1323358000022669)
- Meikle, W. P. S., Allen, D. A., Spyromilio, J., & Varani, G. F. 1989, *MNRAS*, 238, 193, doi: [10.1093/mnras/238.1.193](https://doi.org/10.1093/mnras/238.1.193)
- Meikle, W. P. S., Spyromilio, J., Allen, D. A., Varani, G. F., & Cumming, R. J. 1993, *MNRAS*, 261, 535, doi: [10.1093/mnras/261.3.535](https://doi.org/10.1093/mnras/261.3.535)
- Meikle, W. P. S., Mattila, S., Pastorello, A., et al. 2007a, *ApJ*, 665, 608, doi: [10.1086/519733](https://doi.org/10.1086/519733)
- . 2007b, *ApJ*, 665, 608, doi: [10.1086/519733](https://doi.org/10.1086/519733)
- Muller, E., Hillebrandt, W., Orio, M., et al. 1989, *A&A*, 220, 167
- Nagataki, S., Shimizu, T. M., & Sato, K. 1998, *ApJ*, 495, 413, doi: [10.1086/305258](https://doi.org/10.1086/305258)
- Nozawa, T., Kozasa, T., Umeda, H., Maeda, K., & Nomoto, K. 2003, *ApJ*, 598, 785, doi: [10.1086/379011](https://doi.org/10.1086/379011)
- Nozawa, T., Kozasa, T., Tominaga, N., et al. 2008, *ApJ*, 684, 1343, doi: [10.1086/589961](https://doi.org/10.1086/589961)
- Perrin, M. D., Sivaramakrishnan, A., Lajoie, C.-P., et al. 2014, in *Society of Photo-Optical Instrumentation Engineers (SPIE) Conference Series*, Vol. 9143, *Space Telescopes and Instrumentation 2014: Optical, Infrared, and Millimeter Wave*, ed. J. Oschmann, Jacobus M., M. Clampin, G. G. Fazio, & H. A. MacEwen, 91433X, doi: [10.1117/12.2056689](https://doi.org/10.1117/12.2056689)
- Priddy, R. S., Isaak, K. G., McMahon, R. G., Robson, E. I., & Pearson, C. P. 2003, *MNRAS*, 344, L74, doi: [10.1046/j.1365-8711.2003.07076.x](https://doi.org/10.1046/j.1365-8711.2003.07076.x)
- Prochaska, J., Hennawi, J., Westfall, K., et al. 2020, *The Journal of Open Source Software*, 5, 2308, doi: [10.21105/joss.02308](https://doi.org/10.21105/joss.02308)
- Ressler, M. E., Sukhatme, K. G., Franklin, B. R., et al. 2015, *PASP*, 127, 675, doi: [10.1086/682258](https://doi.org/10.1086/682258)
- Rho, J., Geballe, T. R., Banerjee, D. P. K., et al. 2018, *ApJL*, 864, L20, doi: [10.3847/2041-8213/aa777f](https://doi.org/10.3847/2041-8213/aa777f)
- Rho, J., Shahbandeh, M., Hsiao, E., et al. 2019, *The Astronomer's Telegram*, 12897, 1
- Rho, J., Evans, A., Geballe, T. R., et al. 2021, *ApJ*, 908, 232, doi: [10.3847/1538-4357/abd850](https://doi.org/10.3847/1538-4357/abd850)
- Rieke, G. H., Su, K., Sloan, G. C., & Schlawin, E. 2022, *AJ*, 163, 45, doi: [10.3847/1538-3881/ac3b5d](https://doi.org/10.3847/1538-3881/ac3b5d)
- Rieke, G. H., Wright, G. S., Böker, T., et al. 2015, *PASP*, 127, 584, doi: [10.1086/682252](https://doi.org/10.1086/682252)
- Sarangi, A., & Cherkneff, I. 2015, *A&A*, 575, A95, doi: [10.1051/0004-6361/201424969](https://doi.org/10.1051/0004-6361/201424969)
- Sarangi, A., Matsuura, M., & Micellotta, E. R. 2018, *SSRv*, 214, 63, doi: [10.1007/s11214-018-0492-7](https://doi.org/10.1007/s11214-018-0492-7)
- Schneider, R., Ferrara, A., & Salvaterra, R. 2004, *MNRAS*, 351, 1379, doi: [10.1111/j.1365-2966.2004.07876.x](https://doi.org/10.1111/j.1365-2966.2004.07876.x)
- Shahbandeh, M., Hsiao, E. Y., Ashall, C., et al. 2022, *ApJ*, 925, 175, doi: [10.3847/1538-4357/ac4030](https://doi.org/10.3847/1538-4357/ac4030)
- Shahbandeh, M., Sarangi, A., Temim, T., et al. 2023, *MNRAS*, 523, 6048, doi: [10.1093/mnras/stad1681](https://doi.org/10.1093/mnras/stad1681)
- Sharp, C. M., & Hoeflich, P. 1990, *Ap&SS*, 171, 213, doi: [10.1007/BF00646849](https://doi.org/10.1007/BF00646849)
- Sharp, C. M., & Höflich, P. 1989, *Highlights of Astronomy*, 8, 207
- Sluder, A., Milosavljević, M., & Montgomery, M. H. 2018, *MNRAS*, 480, 5580, doi: [10.1093/mnras/sty2060](https://doi.org/10.1093/mnras/sty2060)
- Spyromilio, J., Meikle, W. P. S., Learner, R. C. M., & Allen, D. A. 1988, *Nature*, 334, 327, doi: [10.1038/334327a0](https://doi.org/10.1038/334327a0)
- Szalai, T., Vinkó, J., Könyves-Tóth, R., et al. 2019, *ApJ*, 876, 19, doi: [10.3847/1538-4357/ab12d0](https://doi.org/10.3847/1538-4357/ab12d0)
- Tartaglia, L., Sand, D. J., Valenti, S., et al. 2018, *ApJ*, 853, 62, doi: [10.3847/1538-4357/aaa014](https://doi.org/10.3847/1538-4357/aaa014)
- Tinyanont, S., Kasliwal, M. M., Krafton, K., et al. 2019, *ApJ*, 873, 127, doi: [10.3847/1538-4357/ab0897](https://doi.org/10.3847/1538-4357/ab0897)
- Todini, P., & Ferrara, A. 2001, *MNRAS*, 325, 726, doi: [10.1046/j.1365-8711.2001.04486.x](https://doi.org/10.1046/j.1365-8711.2001.04486.x)
- Turatto, M., Cappellaro, E., Benetti, S., & Danziger, I. J. 1993, *MNRAS*, 265, 471, doi: [10.1093/mnras/265.2.471](https://doi.org/10.1093/mnras/265.2.471)
- Virtanen, P., Gommers, R., Oliphant, T. E., et al. 2020, *Nature Methods*, 17, 261, doi: [10.1038/s41592-019-0686-2](https://doi.org/10.1038/s41592-019-0686-2)
- Wooden, D. H., Rank, D. M., Bregman, J. D., et al. 1993, *ApJS*, 88, 477, doi: [10.1086/191830](https://doi.org/10.1086/191830)
- Woosley, S. E., Heger, A., & Weaver, T. A. 2002, *Reviews of Modern Physics*, 74, 1015, doi: [10.1103/RevModPhys.74.1015](https://doi.org/10.1103/RevModPhys.74.1015)